scientific reports

OPEN

Thin film flow and heat transfer of Cu-nanofluids with slip and convective boundary condition over a stretching sheet

Azeem Shahzad[1], Fakhira Liaqat[1], Zaffer Ellahi[1], Muhammad Sohail[2✉], Muhammad Ayub[3] & Mohamed R. Ali[4,5✉]

The flow and heat transfer in thin film of Cu-nanofluid over a stretching sheet by considering different shape factors (platelets, blades, bricks, sphere and cylinder) along with slip and convective boundary conditions is investigated. The governing partial differential equations are converted to nonlinear ordinary differential equations by means of suitable similarity transformation and then solved by using BVP4C in MATLAB. The physical significance of various parameters on velocity and temperature profiles are investigated and provided in the form of table and also presented graphically. It is noted that the Platelet-shaped nanoparticles has the highest heat transfer rate as compare to other particle's shapes.

List of symbols

$u_1^*(x, y), u_2^*(x, y)$	Velocities components(m/s)
β	Thickness of film (–)
b	Constants (S^{-1})
u_w	Velocity of surface (m/s)
T_s	Temperature of surface (K)
T_r	Reference temperature (K)
T_o	Slit's temperature (K)
k_f^*	Base fluid's thermal conductivity (W/K/m)
k_{nf}^*	Nanofluid's thermal conductivity (W/K/m)
c_p^*	Fluid's specific heat (J/kg/K)
Nu	Nusselt number (–)
Re	Reynold number (–)
Pr	Prandtl number (–)
B_o	Magnetic field
η	Similarity variable
φ	Nanoparticle's Volume fraction
α_f^*	Thermal diffusivity of water
α_{nf}^*	Thermal diffusivity of nanofluid
ρ_f^*	Density of base fluid (water)
ρ_{nf}^*	Density of nanofluid
μ_f^*	Dynamic viscosity of water
μ_{nf}^*	Dynamic viscosity of nanofluid
ν_f	Kinematic viscosity of water
ν_{nf}	Kinematic viscosity of nanofluid

[1]Basic Sciences Department, University of Engineering and Technology, Taxila 47050, Pakistan. [2]Institute of Mathematics, Khwaja Fareed University of Engineering and Information Technology, Rahim Yar Khan 64200, Pakistan. [3]Department of Mathematics, COMSATS University, Islamabad, Abbottabad Campus, Abbottabad, Pakistan. [4]Faculty of Engineering and Technology, Future University, Cario, Egypt. [5]Department of Mathematics, Benha Faculty of Engineering, Benha University, Benha, Egypt. ✉email: muhammad_sohail111@yahoo.com; mohamed.reda@fue.edu.eg

1

σ_f^*	Electrical conductivity
$(\rho^* C_p^*)_{nf}$	Heat capacity of nanofluid

Nanometer-sized metal particles have been manufactured using new technologies, leading in the development of a new class of fluid known as nanofluids. The mixing of extremely fine metallic particles (or smaller) in a saturated liquid, referred to as nanoparticles, is referred to as two-phase mixture. These fluids have a thermal conductivity that is significantly larger than that of the base fluid[1–3]. Nanofluids have been discovered to have improved thermal physical properties when compared to basic fluids. Nanofluids offer an alternative heat transfer medium, particularly at the micro and nanoscaled, where large heat fluxes are required. Despite their extraordinary potential and qualities, these exceedingly unique fluids are still in their infancy. Much of the early and scant experimental effort focused the determination of nanofluids' effective heat conductivity and dynamic viscosity[4,5]. Xuan and Roetzel[6] studied the heat transport capacity of a nanofluid that changes due to the suspension of ultrafine particles, revealing a significant potential for improving heat transmission.

Copper nanoparticles made of metals have a wide range of applications in heat transfer, electronics, medicine, optics, and the production of antibacterial agents, nanofluids, and lubricants, among others. Due to the high reactivity of copper nanoparticles, oxidation occurs easily. Stabilization of pure copper metal nanoparticles is not achievable. Copper undergoes changes in its structural and thermal properties when it is oxidized to copper oxide. To avoid oxidation, a protective coating on the nanoparticles is utilized. The metallic particles are encapsulated using a variety of inorganic or organic chemicals[7,8].

Heat transfer occurs naturally around us as a result of temperature differences, a process called natural convection. For example, sunlight heats water in rivers and on land. Additionally, fires, tectonic plates, and volcanic hot air are also instances of natural convective heat[9–11]. Sohail and Naz[12] used Cattaneo-Christov theory to analyze the Sutterby nanofluid across a stretched cylinder. They discovered that increasing the magnetic parameter increases the temperature and concentration of the fluid, while having the opposite effect on velocity.

The phrase 'thin film' is frequently used to refer to flow that is defined by the fact that the flow domain in one dimension is significantly smaller than the flow domain in the other (one or two) dimensions. Flow difficulties in thin films are of critical practical importance. The notion of thin film is applied in a wide variety of industrial processes, including lubrication, surface coating, cooling of heat exchanger fins, and contact lens movement[13–15]. Khaled and Vafai[16] examined the flow and temperature distribution within thin films by taking internal and exterior pressure pulsations into account. Bilal et al.[17] used boundary layer theory to examine the heat transport and MHD Darcy-Forchheimer flow of a Sutterby fluid past a linearly stretched boundary. They noticed that when slip increases, magnetic parameters diminish the velocity profile, and a similar trend is evident for fluid temperature as thermal relaxation and slip parameters increase. Marzougui et al.[18] investigated the formation of entropy in convective Cu/H_2O nanofluid flow in a cavity containing Chamfers when a magnetic field was applied. They concluded that increasing the Hartman number decreases viscosity and thermal irreversibility.

Numerous researchers have discussed heat transfer analysis for thin film flow caused by stretching phenomena in non-Newtonian fluids, taking into account various effects such as magnetic field and porous medium, for both steady and unsteady flows; see, for example[19–32], and the references therein. Tiwari and Das[32] investigated the effect of relevant parameters on the heat transmission characteristics of nanofluids inside a heated square form cavity with a two-sided lid. They discovered that by incorporating nanoparticles into a base fluid, they were able to increase the base fluid's heat transfer capacity. Additionally, when solid volume fraction is used, the difference in the average Nusselt number is nonlinear. Naseem et al.[33] investigated the three-dimensional flow properties and heat transfer of a $TiO_2 - Cu/water$ nanofluid travelling across a bidirectional surface using the Tiwari and Das model and the nanofluid's thermophysical parameters. Additionally, higher Eckert and Prandtl values indicate a lower thermal profile. Shahrestani et al.[34] examined laminar Al_2O_3/water nanofluid flow with a constant heat flux to the outer wall of an axisymmetric microchannel while maintaining adiabatic conditions at both ends. This was accomplished by taking only half of the axisymmetric microchannel into account and rotating the domain around its axis. They argued that raising the entrance velocity increases the rate of viscous dissipation and raises the temperature of the wall compared to the fluid's bulk temperature. Thus, the thermal behaviour of the fluid in microchannel is markedly different than in microchannel. Waini et al.[35] examined the flow of a nanofluid toward a shrinking cylinder of Al_2O_3 nanoparticles. They determined that the first solution is stable. Afridi et al.[36] investigated the flow and heat transfer properties of traditional and hybrid nanofluids. They investigated the development of entropy in conventional and hybrid nanofluid flows. Both nanofluids were considered to flow with heat dissipation along a narrow needle. They discovered that the hybrid nanofluid exhibited a more elevated temperature profile than the conventional nanofluid. Abbas et al.[37] used a horizontal Riga plate to investigate the production of entropy in viscous nanofluids. Shankaralingappa et al.[38] discussed the flow, heat and mass transfer by taking nonlinear fluid flow over stretching sheet by using Cattaneo–Christov heat flux model. The concentration profile drops as the thermophoretic and chemical reaction rate parameters increase in value. Many researcher work on stretching surfaces and analyze the different effects which can be seen in[38–45].

To the authors' knowledge, no study has been conducted to investigate the effect of various shapes of Cu-nanofluid, such as sphere, cylinder, platelet, blade, and brick, on thin film flow and heat transfer over a stretching sheet with magnetic effect and convective boundary condition and partial slip, using water as the base fluid. The effect on temperature and velocity distributions of physical quantities, like, the volume fraction φ of nanofluids the unsteadiness parameter S, the Prandtl number (Pr), is carried out.
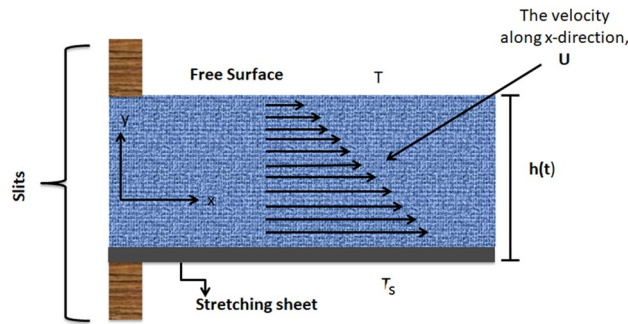
Figure 1. The flow of nanofluid composed by multi-nanomaterial.

Mathematical method and formulation

In this investigation a 2-D unsteady, incompressible, a liquid thin film flow of Cu/H_2O nanofluid past a stretchable sheet which is positioned along x-axis is considered as shown in Fig. 1. Thin film flow emerges because of the stretching of sheet. Thickness of the liquid film is $h(t)$, while the surface temperature and velocity of the stretching sheet, denoted by U_w and T_s respectively. The horizontal velocity is $U_w(x, t) = \frac{bx}{1-\alpha t}$, ($a$ and b are constants) and the wall temperature distribution is determined by:

$$T_s = T_o - T_r \left(\frac{bx^2}{2v_f} \right)(1 - \alpha t)^{-\frac{3}{2}}$$

The constant reference temperature and the temperature of the slit are respectively given as T_r and T_0, whereas, v_f^* is the kinematics viscosity of fluid. The perpendicular magnetic field (uniform) of strength $B(t) = \frac{B_0}{\sqrt{1-\alpha t}}$ to the stretching layer is applied.

By using the Tiwari and Das model[26] for nanofluid the governing continuity, momentum, and energy equations are given as

$$\frac{\partial u_1^*}{\partial x} + \frac{\partial u_2^*}{\partial y} = 0, \tag{1}$$

$$\frac{\partial u_1^*}{\partial t} + u_1^* \frac{\partial u_1^*}{\partial x} + u_2^* \frac{\partial u_1^*}{\partial y} = \frac{\mu_{nf}^*}{\rho_{nf}^*} \frac{\partial^2 u_1^*}{\partial^2 y} - \frac{\sigma_{nf}^*}{\rho_{nf}^*} B(t)^2 u_1^*, \tag{2}$$

$$\frac{\partial T^*}{\partial t} + u_1^* \frac{\partial T^*}{\partial x} + u_2^* \frac{\partial T^*}{\partial y} = \alpha_{nf}^* \frac{\partial^2 T^*}{\partial^2 y} + \frac{\mu_{nf}}{\rho_{nf}^* C_p^*} \left(\frac{\partial u_1^*}{\partial y} \right)^2, \tag{3}$$

where $u_1^*(x, y, t)$ and $u_2^*(x, y, t)$, are velocities and $T^*(x, y, t)$ represents the temperature. For present analysis, the boundaries conditions are

$$u_1^* = U_w + Av_f^* \frac{\partial u^*}{\partial y}, u_2^* = \frac{dh^*}{dt}, -k_{nf}^* \frac{\partial T^*}{\partial y} = h_f^*(T_o - T^*), \text{ at y} = 0, \tag{4}$$

$$\frac{\partial u_1^*}{\partial y} = \frac{\partial T^*}{\partial y} = 0, u_2^* = \frac{dh^*}{dt}, \text{ at y} = h^*(t), \tag{5}$$

where slip parameter and convective heat transfer coefficients of proportionality are A and h_f^* respectively. Thermo-physical properties such as $\mu_{nf}^*, \sigma_{nf}^*, \rho_{nf}^*, (\rho^* C_p^*)_{nf}$, and α_{nf}^* are dynamic viscosity, electrical conductivity, density, and heat capacity, and diffusivity of the nanofluid respectively, mathematically given by[28,29]

$$\alpha_{nf}^* = \frac{k_{nf}^*}{(\rho^* C_p^*)_{nf}}, \rho_{nf}^* = (1 - \varphi)\rho_f^* + \varphi\rho_s^*, \mu_{nf}^*$$

$$= \mu_f^* \left(1 + A_1^* \varphi + A_2^* \varphi^2 \right),$$

$$\sigma_{nf}^* = \sigma_f^*(1 - \varphi)\sigma_f^* + \varphi\sigma_s^*, \left(\rho^* C_p^* \right)_{nf}$$

$$= (1 - \varphi)(\rho^* C_p^*)_f + \varphi(\rho^* C_p^*)_s, \tag{6}$$

and

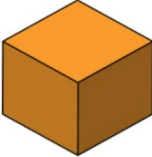| Nanoparticle and Base fluid	Thermal Conductivity (W/mK)	Density $\left(Kg/m^3\right)$	Electrical Conductivity (S/m)	Specific heat (J/KgK)
Cu	401	8933	59.6	385
H_2O	0.613	97.19	5.50	4179

Table 1. Thermophysical characteristics of H_2O/Cu[13].
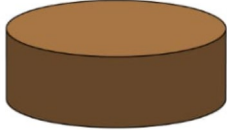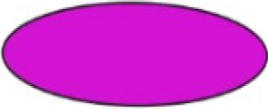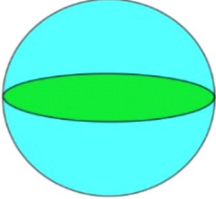
Nanoparticle's shape	A1	A2	m
Platelet	37.1	612.6	5.72
Cylinder	13.5	904.4	4.82
Blade	14.6	123.3	8.26
Brick	1.9	471.4	3.72
Sphere	2.5	6.5	3.0

Table 2. Heat capacitance coefficients, size, and nanoparticle's shapes[14].

$$\frac{k_{nf}^*}{k_f^*} = \left[\frac{k_s^* + (m-1)k_f^* + (m-1)\left(k_s^* - k_f^*\right)\varphi}{k_s^* + (m-1)k_f^* + \left(k_s^* - k_f^*\right)\varphi}\right], \tag{7}$$

where the volume fraction of the nanofluid is denoted by φ. The viscosity enhancement heat capacitance coefficients are A_1^*, A_2^* and the heat power is expressed by $(\rho^* C_p^*)_{nf}$. Furthermore, k_s^* and m, are thermal conductivity and size of the nanoparticle while thermophysical properties of base fluid, nanofluid, and nanoparticles are respectively displayed by subscripts f, nf, and s. In addition, the thermophysical properties of base fluid and nanoparticle are shown in Table 1 and properties regarding shape factors are mentioned in Table 2. Defining transformations of resemblance, as

$$T_s = T_\circ - T_r\left(\frac{bx^{*2}}{2v_f}\right)(1 - \alpha t)^{-\frac{3}{2}}\theta(\eta), \quad \eta = \left(\frac{b}{v_f^*(1 - \alpha t)}\right)^{\frac{1}{2}}, \quad \psi = \left(\frac{bv_f^*}{1 - \alpha t}\right)^{\frac{1}{2}} xf(\eta), \tag{8}$$

where stream function ψ determine the pattern of flow and is defined as $u_1^* = \frac{\partial \psi}{\partial y}$ and $u_2^* = -\frac{\partial \psi}{\partial x}$, so that equation of continuity is satisfied identically. By substituting the above defined dimensionless variables Eq. (8) into Eqs. (2–3), the following nonlinear ODEs are obtained. Also by using (8) in (4, 5) the transformed boundary conditions becomes

$$\varepsilon_1 f'''(\eta) - \varepsilon_3 M f'(\eta) + \left[f(\eta) f''(\eta) - f'^2(\eta) - S\left(f'(\eta) + \frac{\eta}{2} f''(\eta) \right) \right] = 0, \tag{9}$$

$$\frac{\varepsilon_2}{Pr} \theta''(\eta) + \varepsilon_1 E_c f''^2(\eta) + \left[f(\eta) \theta'(\eta) - 2\theta(\eta) f'(\eta) - \frac{S}{2} \left(3\theta(\eta) + + \eta \theta'(\eta) \right) \right] \tag{10}$$

and

$$f(0) = 0, \; f'(0) = 1 + K f''(0), \; \theta'(0) = -\frac{k_f}{k_{nf}} \gamma (1 - \theta(0)),$$

$$f(\beta) = \frac{S\beta}{2}, \; f''(\beta) = 0, \; \theta'(\beta) = 0. \tag{11}$$

The dimensionless constants $K = A\sqrt{\frac{v_f^* U_w}{x}}$, $E_c = \frac{U_w^2}{C_p^*(T_s - T^*)}$, $M = \frac{\beta_0^2 \sigma_f^*}{b \rho_{nf}^*}$, $Pr = \frac{\rho^*(C_p^*)_f v_f^*}{k_f^*}$ and $S = \frac{a}{b}$ are slip parameter, Eckert number, magnetic parameter, Prandtl number and unsteadiness parameter respectively. Additionally, $\varepsilon_i, \; i = 1, ..., 3$ are constants and described as

$$\varepsilon_1 = \frac{1 + A_1^* \varphi + A_2^* \varphi^2}{1 - \varphi + \varphi \left(\frac{\rho_s^*}{\rho_f^*} \right)}, \varepsilon_2 = \frac{\frac{k_{nf}^*}{k_f^*}}{1 - \varphi + \varphi \frac{(\rho^* C_p^*)_s}{(\rho^* C_p^*)_f}}, \varepsilon_3 = \frac{1 - \varphi + \varphi \left(\frac{\sigma_s^*}{\sigma_f^*} \right)}{1 - \varphi + \varphi \left(\frac{\rho_s^*}{\rho_f^*} \right)}, \tag{12}$$

where φ^* is the solid volume-fraction. Skin shear stress and heat transfer coefficient are described as

$$C_f = \frac{\tau_w}{\rho_f^* U_w^2} \text{ and } Nu = \frac{x^* q_w}{k_f^*(T_s - T_0)},$$

where $\tag{13}$

$$\tau_w = \mu_{nf}^* \left[\frac{\partial u_1^*}{\partial y^*} \right]_{y^*=0}, q_w = -k_{nf}^* \left[\frac{\partial T^*}{\partial y^*} \right]_{y^*=0}.$$

The non-dimensional form of Eq. (13) with respect to transformed variables is

$$C_f = \frac{\left(1 + A_1^* \varphi + A_2^* \varphi^2\right)}{Re^{\frac{1}{2}}} f''(0), \; Re^{\frac{-1}{2}} Nu = -\frac{k_{nf}^*}{k_f^*} \theta'(0). \tag{14}$$

Solutions of the problem

By using the similarity transformation, non-linear PDEs with boundary conditions are transformed into non-linear ODEs. Here, these non-linear ODEs have been reduced to first order ordinary differential equations as

$$y_1 = f, \; y_1' = y_2, \; y_2' = y_3, \tag{15}$$

$$y_3' = \frac{\varepsilon_3}{\varepsilon_1} + M y_2 - \frac{1}{\varepsilon_1} \left[y_1 y_3 - y_2^2 - S\left(y_2 + \frac{\eta}{2} y_3 \right) \right], \tag{16}$$

$$\theta = y_4, y_4' = y_5$$

$$y_5' = -\frac{\varepsilon_1}{\varepsilon_2} Pr E_c y_3^2 - \frac{1}{\varepsilon_2} \left[y_1 y_5 - 2 y_4 y_2 - \frac{S}{2} (3 y_4 + \eta y_4) \right], \tag{17}$$

$$y_1(0) = 0, y_2(0) = 1 + K y_3(0), y_5(0) = -\gamma \left(1 - y_4(0) \right), \tag{18}$$

$$y_2(\beta) = \frac{S\beta}{2}, y_3(\beta) = 0, y_5(\beta) = 0. \tag{19}$$

The extraneous condition $y_2(\beta) = \frac{S\beta}{2}$ is utilized to evaluate, which is achieved using a hit-and-trial approach. Using BVP4C in MATLAB, the coupled ODE system is solved for the known values of S and β. The flow chart is shown in Fig. 2.
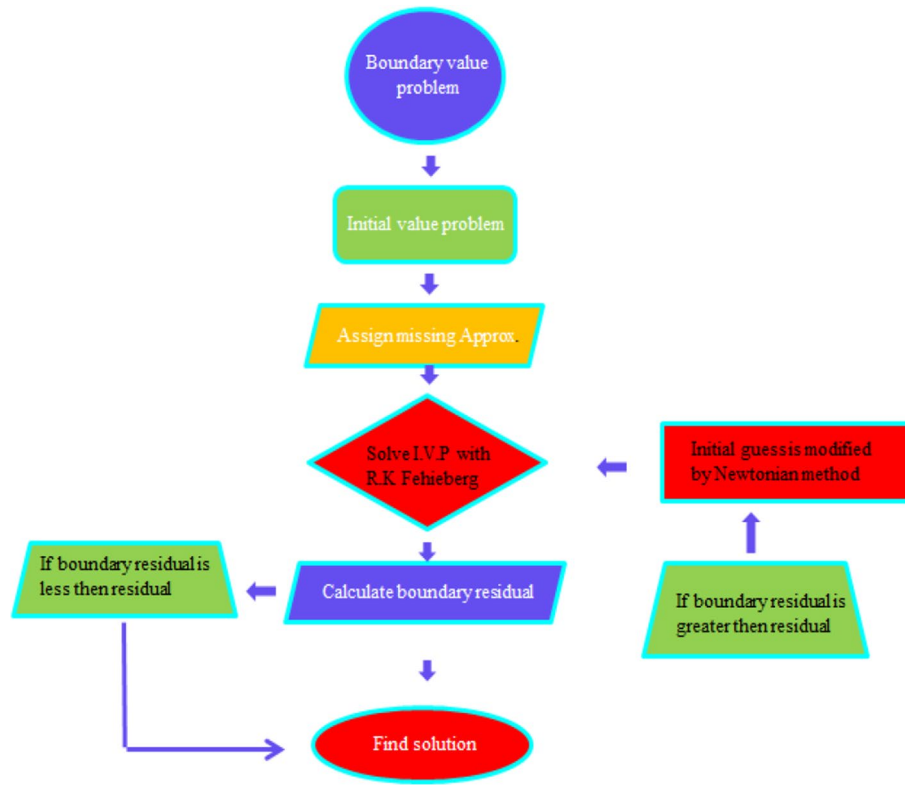
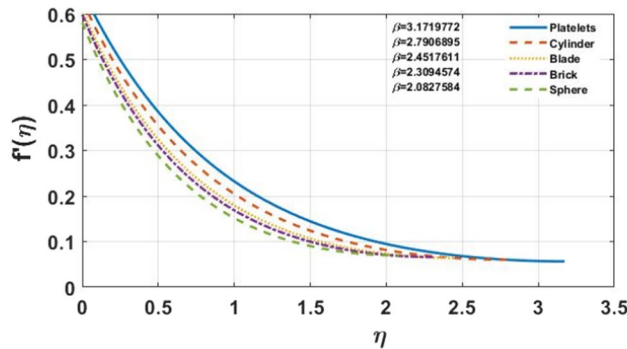**Figure 2.** Flow chart related to numerical scheme.

Figure 3. The impact of shape of nanoparticle on $f'(\eta)$, for $\varphi = 0.02, S = 0.4, K = 0.5, M = 1.0$.

Numerical results and discussion

The physical flow quantities, Eckert number (Ec), Prandtl number (Pr), Biot number (γ), unsteadiness parameter S, and magnetic field strength (M) are crucial in the temperature, velocity, and local heat transfer rate for the physical problem under consideration. In this section numerical results derived for solving Eqs. (9–11) with BVP4C approach. The change in different shapes of nanoparticles in nanofluid thin film over stretched layer influences both temperature and velocity profiles. The enhanced thermal conductivity of the base fluid due to increase in volume fraction of base fluid, nanoparticles boost the heat of the base fluid. The high concentration of nanoparticles in the thermal boundary layer on the wall side, which can be explained by nanoparticle migration, is one of the reasons for improved nanofluid heat transfer. It should also be observed that as the volume fraction grows, so does the thickness of the thermal boundary layer. The increase in shear stress and skin friction leads the nanofluids speed to drop towards the end.

The impact of different shapes of nanoparticles on the film thickness β of Cu-nanofluids is shown in Fig. 3, while other physical parameters are held constant. The thickness of the film was substantially changed by varying the shapes of the nanoparticles. Although the fact that the film thickness value increases for platelet nano-sized
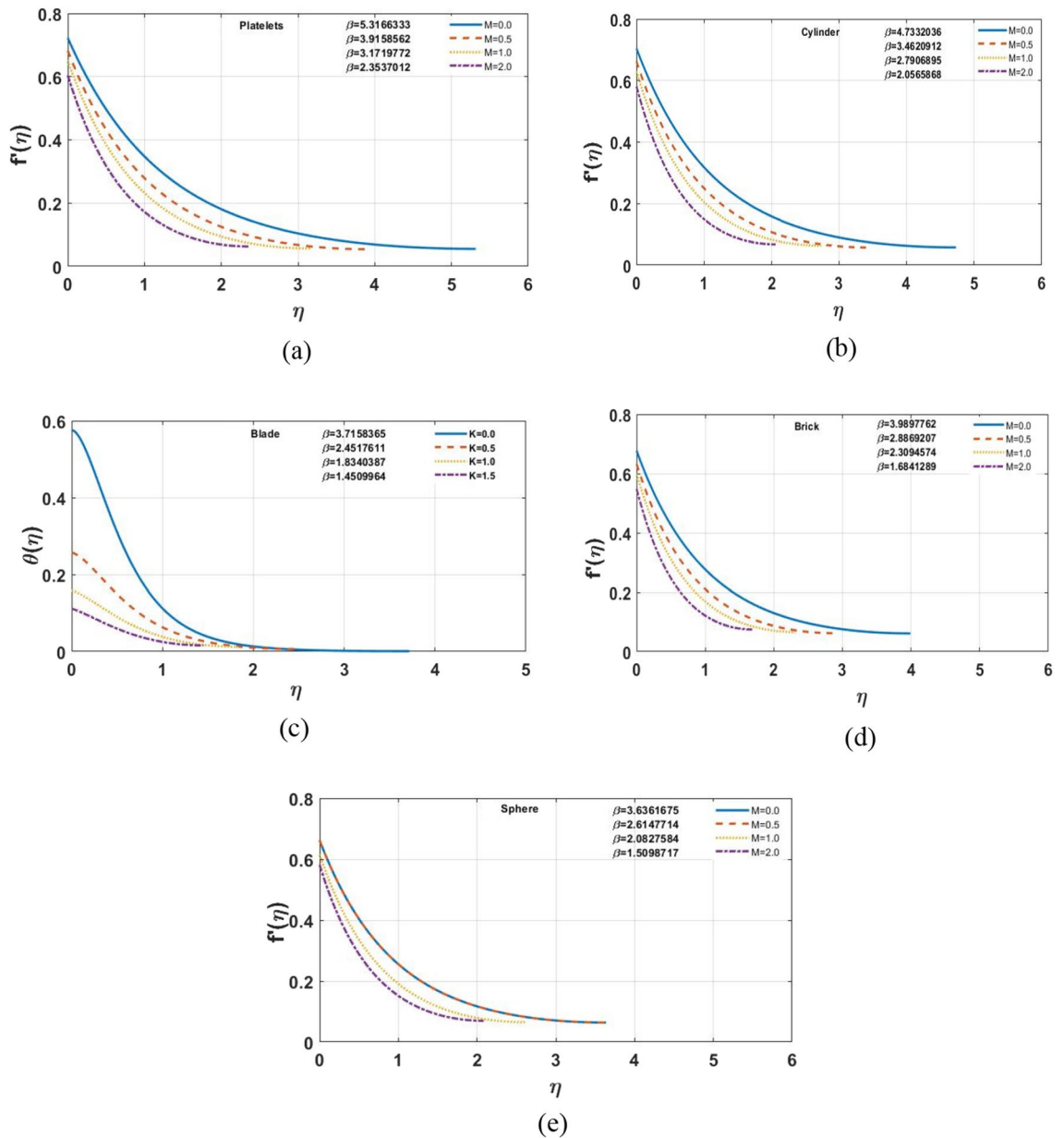
Figure 4. (**a–e**) Effects of Slip parameter M on the velocity profile for S = 0.4, K = 0.5 and φ = 0.02.

particles and lowers for other forms of nanoparticles such as blade, cylinder, brick, and sphere comparatively. The impact of the magnetic parameter M on different shapes of nanoparticles displayed in the Fig. 4a–e. It is observed that as the value of M increases, the velocity profile for each multi-shape nanoparticle decreases. The impact of the slip parameter k on different shapes of nanoparticles displayed in the Fig. 5a–e. It is observed that as the value of K drops, the temperature profile for each multi-shape nanoparticle diminishes. With higher values of parameter K, the thickness of the film β also decreases. Figure 6a–e shows that better results are obtained in the variation of φ, with a little change in temperature profile for spherical particles. Furthermore, as the thickness of the film β grows, so does the volume-fraction φ parameter.

Figure 7a–e indicates influence of γ on the temperature distribution. For the growing values of γ steadily increase in results can be seen for multi-shape nano-size particles. Moreover, for increasing values of γ temperature also increases. The Biot-number is the ratio of heat convection at the surface to conduction within the surface. As the thermal gradient is introduced to a surface, the temperature inside the surface changes dramatically, while and the surface heats/cools with time. The temperature profile is clearly affected when the value of Ec grows, however, for brick and platelet shaped nanoparticles the temperature distribution is less effected as shown in Fig. 8a–e From physically point of view, Eckert number is based on viscous dissipation whereas concept of viscous dissipation is raised using term work done of particles in view of heat transfer phenomenon. So, an increment in Eckert number results an increment in viscous dissipation. It means that thermal layers are increased when Eckert number is increased. Furthermore, the velocity profile and film thickness increase for
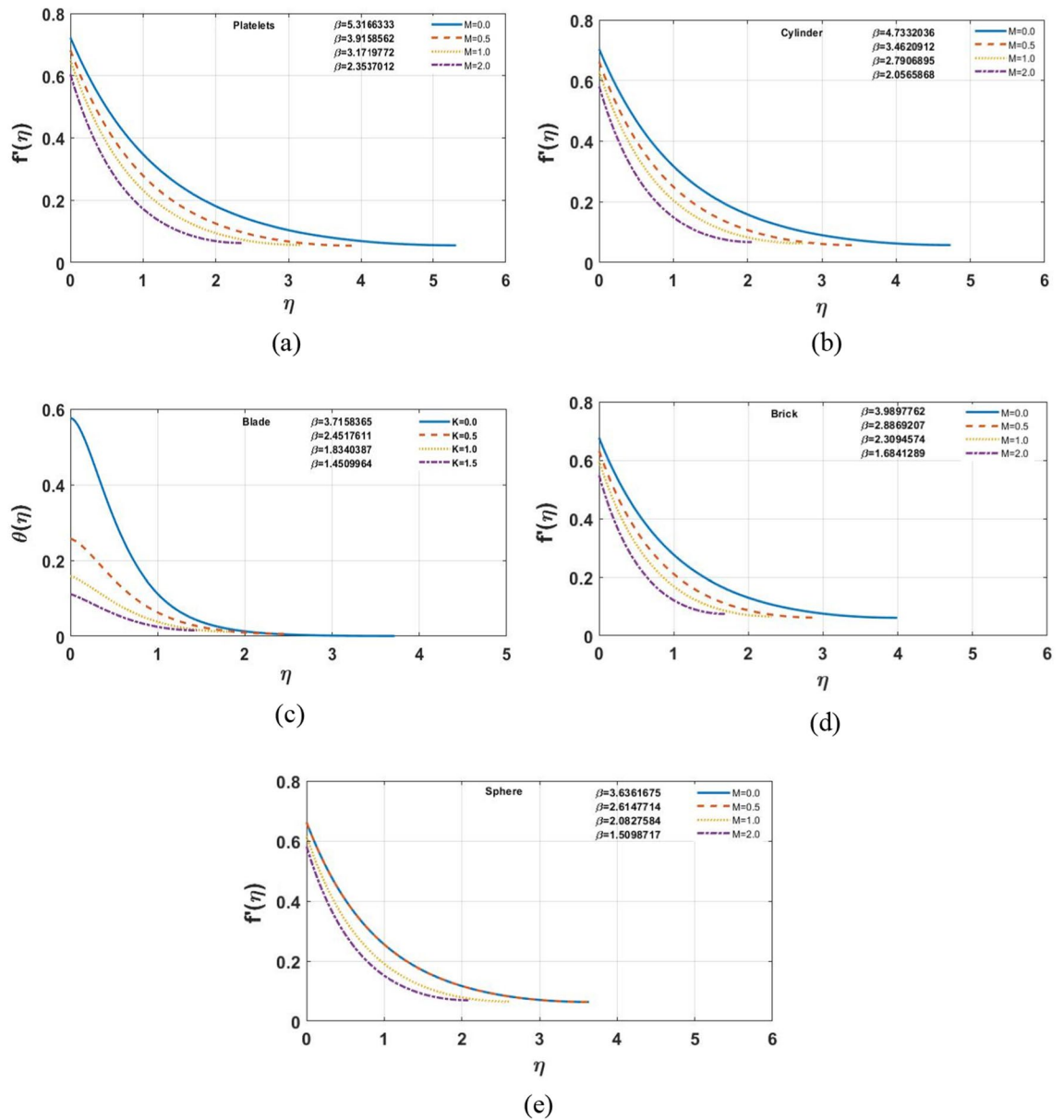
Figure 5. (**a–e**) The impact of S on $\theta(\eta)$, for $S = 0.4$, $M = 1.0$, $\varphi = 0.02$, $\gamma = 0.1$, $Ec = 1.0$, $\mathrm{Pr} = 6.0$.

platelets and decreases for other nano sized particles. The increase in Prandtl number *Pr* decreases the temperature profile shown in Fig. 9a–e. For the larger Prandtl number, the fluids retain weaker thermal diffusivity and conversely. Ratio among thermal and momentum layers makes a Prandtl number and measurement of thermal as well as momentum layers is analyzed using numerical values of Prandtl number. Thickness of thermal layers can be easily controlled by Prandtl number. The reduction in temperature profile produces due to the change in thermal diffusivity. In contrast to platelet shape nanoparticles, change is found for brick shape nanoparticles. In addition, for platelet shape nanoparticles the velocity distribution and the film thickness expedite while reverse behavior is observed for other nanoparticles. The temperature profile for different shapes of nanoparticles is shown in the Fig. 10. It is found that the platelet shape of nanoparticles is highly influential as compare to others.

The numerical results of dimensionless skin-friction coefficient for different shape of nanoparticles are given in Table 3. Decreasing values of skin-friction coefficient are found for increasing values of slip parameter *K* and unsteadiness parameter *S*, whereas the reverse behaviour is noticed in case of magnetic parameter *M* and volume-fraction parameter *φ*.

The thermal transfer rate is also measured and given in Table 4. The increase in Prandtl and Eckert numbers causes decay in the Nusselt number. For increasing value of Biot-number and unsteadiness parameter, increase in Nusselt number is also observed.
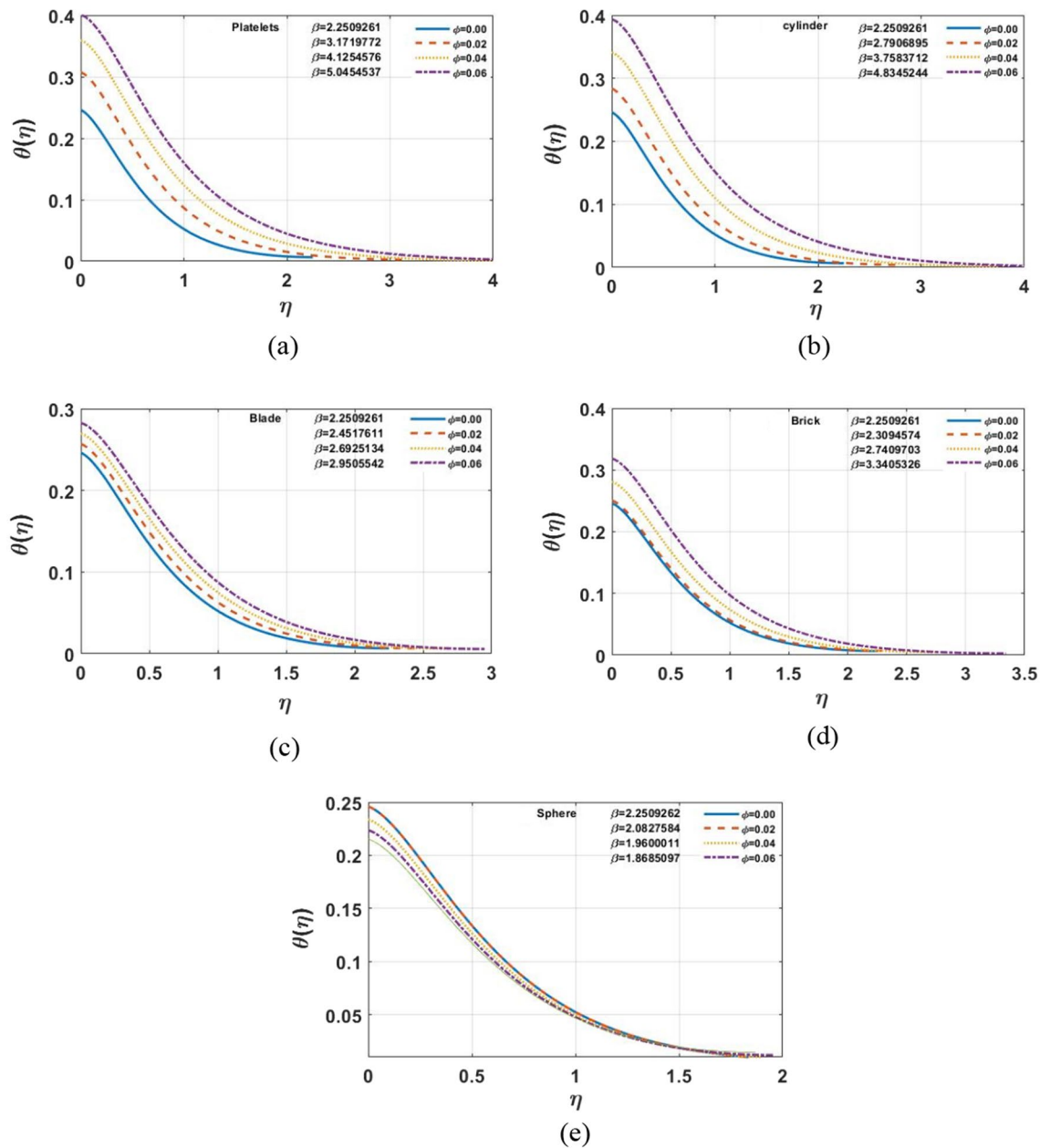
Figure 6. (**a–e**) The impact of φ on $\theta(\eta)$, for $\Pr = 6.0,\ M = 1.0,\ S = 0.4,\ K = 0.5,\ Ec = 1.0,\ \gamma = 0.1$.

The comparison of obtained results with the available literature and given in Table 5 which shows that proposed scheme is accurate and convergent.

Conclusion and key findings

A thermal transport analysis is recorded in nanofluids in the presence of convective boundary conditions and heat generation/absorption for multiple shapes of tiny particles. Over an unsteady thin film, the flow is carried out. The effects on the velocity and temperature behaviour of the main flow parameters are demonstrated.

- Prandtl and Eckert number decreases for slip parameter, but on the other hand unsteadiness parameter, Biot-number, and Nusselt number increases for slip parameter;
- Among the studied particle forms, the velocity of Cu nanofluids consisting of platelet-shaped tiny particles is largest. The Cu nano fluid's velocity profile approaches its minimum for nanoparticles of sphere-shape, while thermal conductivity shows a similar pattern;
- Additionally, as the Biot number γ grows, the temperature $\theta(\eta)$ increases, whereas the value of film thickness β increases for platelet-shaped nanoparticles and drops for cylinder, blade, brick, and sphere-shaped nanoparticles;
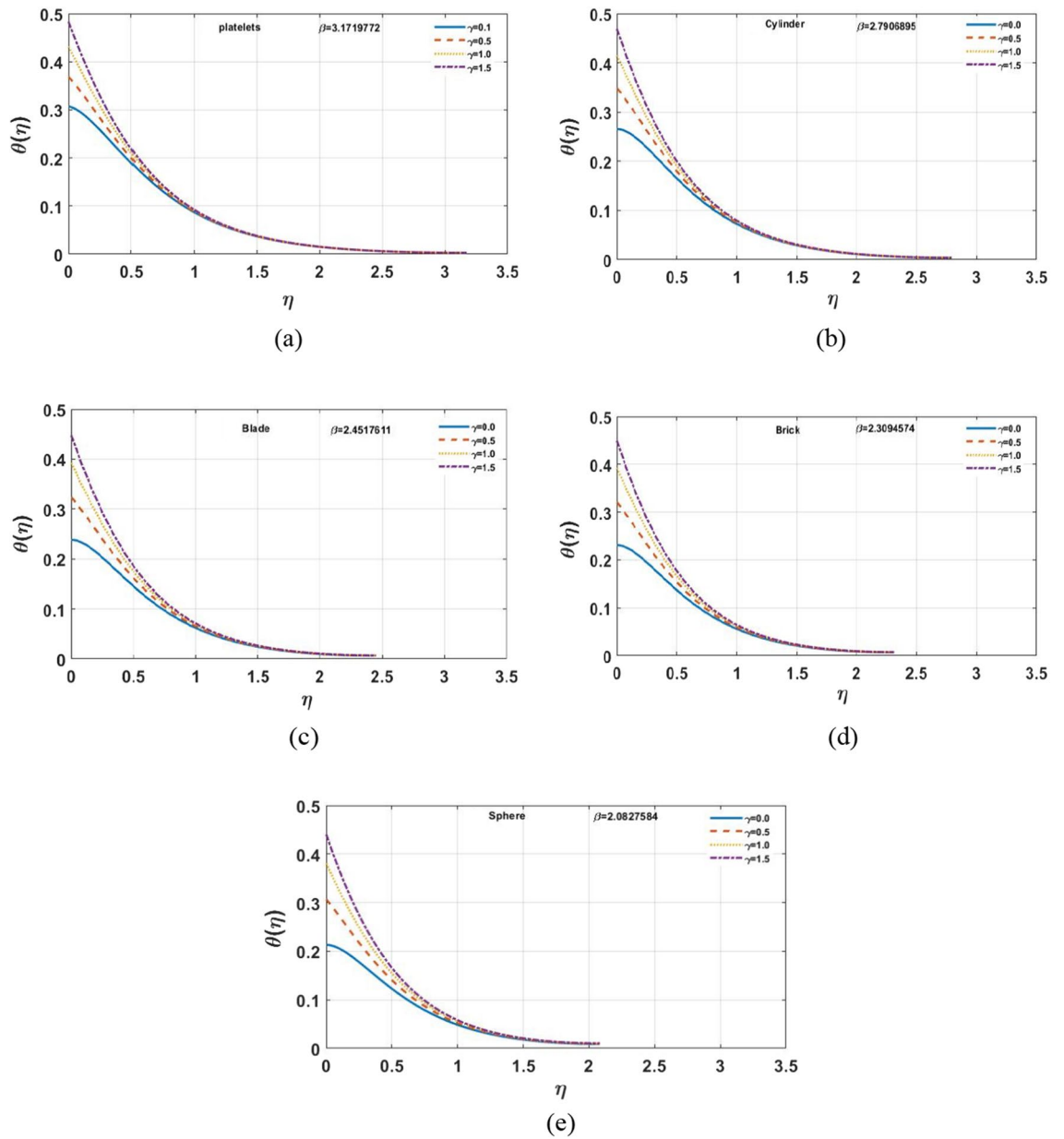
Figure 7. **(a–e)** The impact of γ on $\theta(\eta)$ for $\varphi = 0.02, K = 0.5, \text{Pr} = 6.0, \ Ec = 1.0, S = 0.4, M = 1.0$.
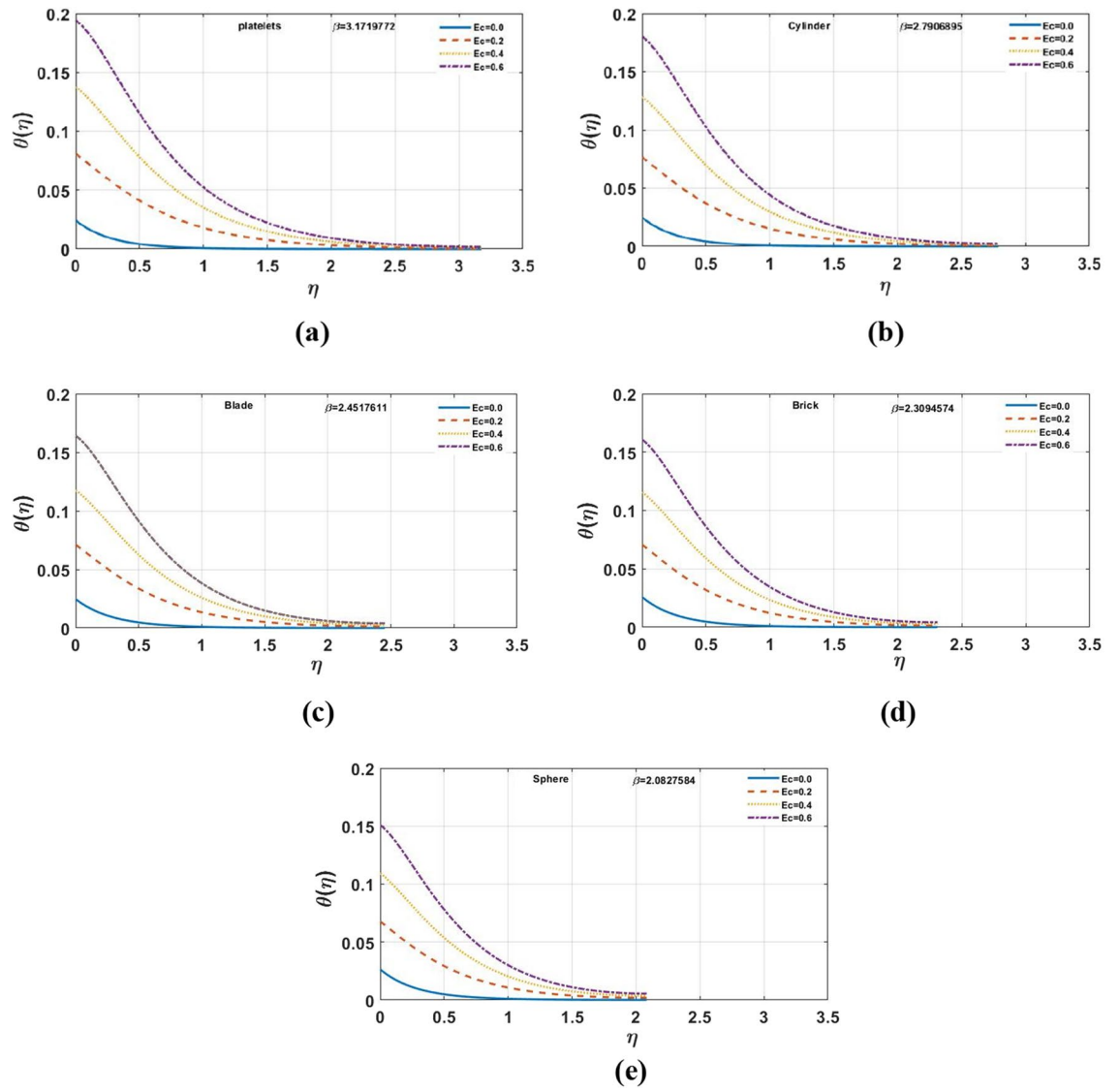
Figure 8. (**a**–**e**) The impact of Ec on $\theta(\eta)$ for $S = 0.4, M = 1.0, \ K = 0.5, \varphi = 0.02, \gamma = 0.1, \text{Pr} = 6.0$.
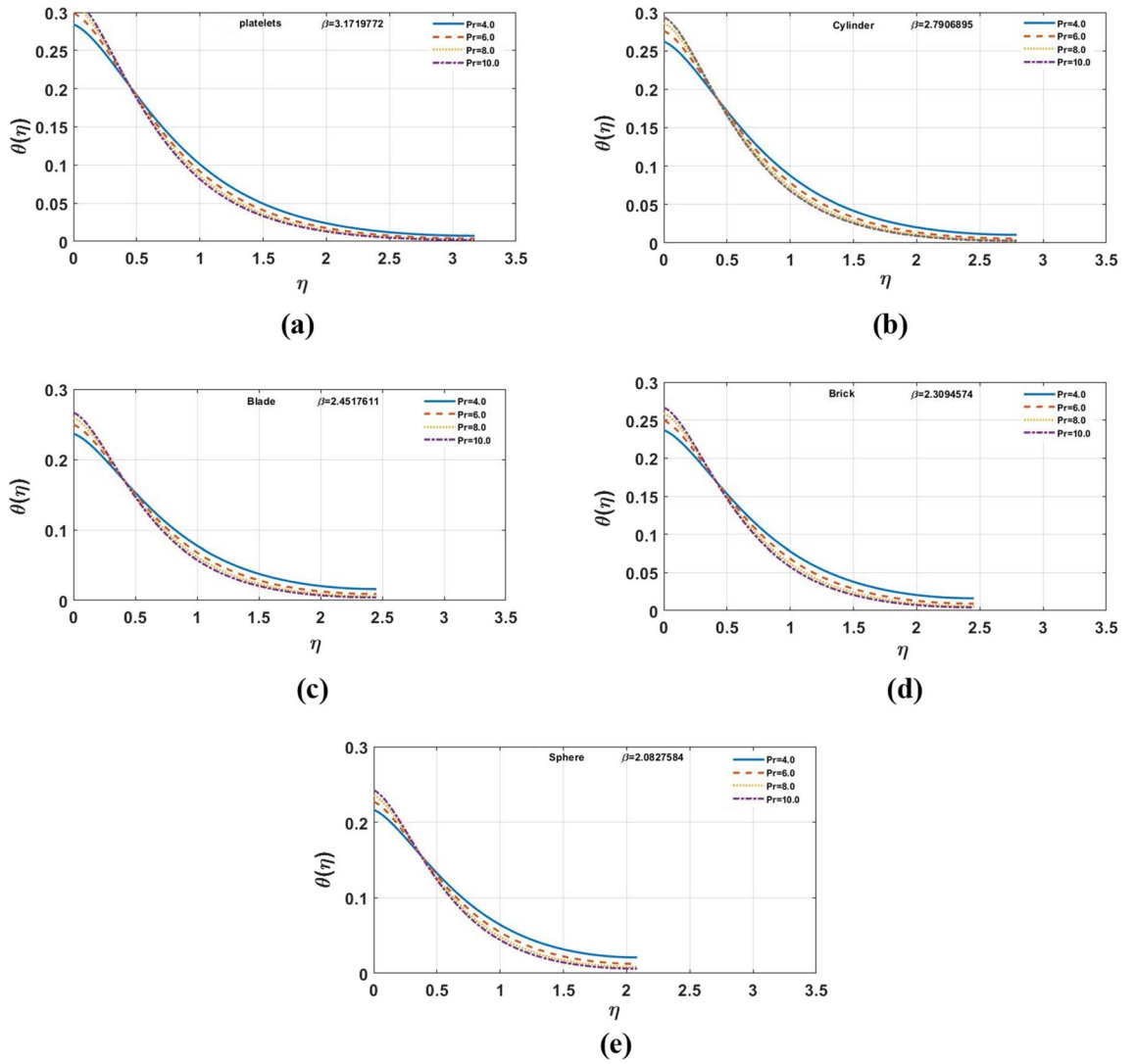
Figure 9. (**a–e**) The impact of Pr on $\theta(\eta)$, for $M = 1.0, \varphi = 0.02, \gamma = 0.1, K = 0.5, S = 0.4, Ec = 1.0$.
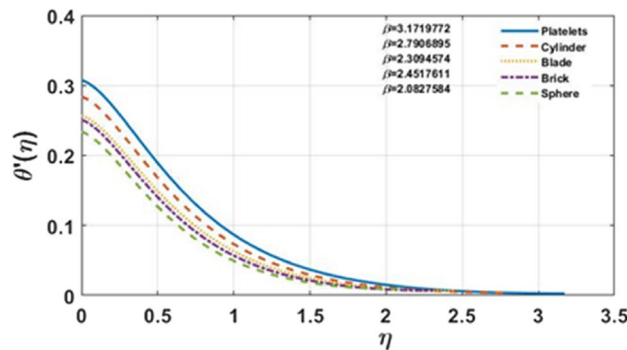

Figure 10. The influence of shape factor on temperature profile, for fixed values of $\varphi = 0.02, M = 1.0, \gamma = 0.1, K = 0.5, S = 0.4, Pr = 6.0, Ec = 1.0$.

Physical parameter				Platelets	Cylinder	Blade	Brick	Sphere
S	M	K	φ	$f''(0)$				
0.4	–	–	–	1.386092	1.207706	1.050703	0.985285	0.881762
0.6	–	–	–	1.371608	1.214893	1.054369	0.987525	0.881803
0.8	–	–	–	1.397411	1.187585	1.026065	0.958923	0.852904
–	0.0	–	–	1.101854	0.964370	0.844057	0.792183	0.711687
–	0.5	–	–	1.262221	1.102173	0.961058	0.902181	0.808897
–	1.0	–	–	1.386092	1.207380	1.050703	0.985285	0.881762
–	2.0	–	–	1.572132	1.364654	1.182631	1.106975	0.987503
–	–	0.0	–	2.314394	2.097308	1.901517	1.814163	1.684479
–	–	0.5	–	1.386092	1.207706	1.050703	0.985285	0.881761
–	–	1.0	–	1.002118	0.859146	0.735391	0.684465	0.604718
–	–	1.5	–	0.785448	0.666745	0.565083	0.523579	0.459017
–	–	–	0.00	0.812143	0.812143	0.812143	0.812143	0.812143
–	–	–	0.02	1.386092	1.207706	1.050703	0.985285	0.881762
–	–	–	0.04	2.118136	1.091649	1.339250	1.365171	0.952327
–	–	–	0.06	2.974656	2.841773	1.673068	1.911689	1.024716

Table 3. The skin-friction coefficient's numerical values for multi-shaped nanoparticles.

Physical parameter						Platelets	Cylinder	Blade	Brick	Sphere
S	K	Φ	Ec	Pr	γ	$-\theta'(0)$				
0.4	0.4	0.02	1.0	7.56	0.1	0.0692554	0.0716217	0.0743009	0.0749311	0.0766112
0.6	–	–	–	–	–	0.0731650	0.0755059	0.0781246	0.0787672	0.0804123
0.8	–	–	–	–	–	0.0780458	0.0803049	0.0827557	0.0833739	0.0848734
–	0.0	–	–	–	–	0.0382963	0.0399336	0.0423572	0.0428332	0.0437179
–	0.5	–	–	–	–	0.0692554	0.0716217	0.0743009	0.0749311	0.0766112
–	1.0	–	–	–	–	0.0801710	0.0820764	0.0841391	0.0846297	0.0858719
–	1.5	–	–	–	–	0.0857099	0.0872269	0.0888311	0.0891859	0.0900966
–	–	0.02	–	–	–	0.0692554	0.0716217	0.0743009	0.0749311	0.0766112
–	–	0.04	–	–	–	0.0640684	0.0658535	0.0730262	0.0718965	0.0776249
–	–	0.06	–	–	–	0.0599186	0.0606182	0.0717395	0.0681422	0.0784721
–	–	–	0.0	–	–	0.0975700	0.0975078	0.0975301	0.0974143	0.0973575
–	–	–	0.2	–	–	0.0919071	0.0923306	0.0928843	0.0929177	0.0932082
–	–	–	0.4	–	–	0.0862442	0.0871534	0.0882384	0.0884210	0.0890589
–	–	–	0.6	–	–	0.0805813	0.0819761	0.0835926	0.0839244	0.0849097
–	–	–	–	4.0	–	0.0715811	0.0737887	0.0763178	0.0768301	0.0783452
–	–	–	–	6.0	–	0.0701116	0.0724280	0.0750631	0.0756529	0.0772808
–	–	–	–	8.0	–	0.0690458	0.0714228	0.0741113	0.0747509	0.0764426
–	–	–	–	10.0	–	0.0682222	0.0706374	0.0733566	0.0740319	0.0757657
–	–	–	–	–	0.5	0.3156011	0.0325645	0.0338102	0.3395379	0.0346438
–	–	–	–	–	1.0	0.5682739	0.5850011	0.6078829	0.6078562	0.6189190
–	–	–	–	–	1.5	0.7751334	0.7964388	0.8281516	0.8252357	0.8388418

Table 4. The numerical results Nusselt number $-\theta'(0)$ for multi-shape nanoparticles.

	Wang[47]		Abel et al.[48]		Li et al.[46]		Present	
S	β	f″(0)	β	f″(0)	β	f″(0)	β	f″(0)
0.4	5.12249	− 1.30778	4.98146	− 1.13409	4.98146	− 1.134	4.98147	− 1.13409
0.6	3.13125	− 1.19516	3.13171	− 1.19513	3.13192	− 1.195	3.13171	− 1.19512
0.8	2.15199	− 1.24579	2.15199	− 1.24580	2.15237	− 1.246	2.15202	− 1.24581
1.0	1.54362	− 1.27776	1.54362	− 1.27777	1.54359	− 1.278	1.54362	− 1.27777
1.2	1.12778	− 1.27918	1.12278	− 1.27917	1.12778	− 1.279	1.12778	− 1.27917
1.4	0.82103	− 1.23355	0.82210	− 1.23354	0.82103	− 1.234	0.82103	− 1.23354
1.6	0.57617	− 1.11494	0.57617	− 1.11494	0.57617	− 1.115	0.57617	1.114937
1.8	0.35639	− 0.86741	0.35639	− 0.86742	0.35639	− 0.8674	0.35639	0.867410

Table 5. The numerical results with the published work for M, K, and $\phi = 0$.

- For slip and unsteadiness parameters, the skin friction coefficient is reduced while the volume-fraction parameter is increased;
- When the slip parameter K is increased the film thickness β is getting reduced;
- Furthermore, for the increase in volume-fraction φ the film thickness β also increases.

Data availability

The datasets generated/produced during and/or analyzed during the current study/research are available from the corresponding author on reasonable request.

References

1. Masuda, H., Ebata, A. & Teramae, K. Alteration of thermal conductivity and viscosity of liquid by dispersing ultra-fine particles. In *Dispersion of Al2O3, SiO2 and TiO2 ultra-fine particles* (1993).
2. Choi, S.U. & Eastman, J.A. Enhancing thermal conductivity of fluids with nanoparticles (No. ANL/MSD/CP-84938; CONF-951135-29). In *Argonne National Lab.*, IL (United States) (1995).
3. Lee, S., Choi, S.S., Li, S.A. & Eastman, J.A. Measuring thermal conductivity of fluids containing oxide nanoparticles (1999).
4. Lee, S. & Choi, S.U. Application of metallic nanoparticle suspensions in advanced cooling systems (No. ANL/ET/CP-90558; CONF-961105-20). In *Argonne National Lab.,* IL (United States) (1996).
5. Mansour, R. B., Galanis, N. & Nguyen, C. T. Effect of uncertainties in physical properties on forced convection heat transfer with nanofluids. *Appl. Therm. Eng.* **27**(1), 240–249 (2007).
6. Xuan, Y. & Roetzel, W. Conceptions for heat transfer correlation of nanofluids. *Int. J. Heat Mass Transf.* **43**(19), 3701–3707 (2000).
7. Wang, X. Q. & Mujumdar, A. S. Heat transfer characteristics of nanofluids: A review. *Int. J. Therm. Sci.* **46**(1), 1–19 (2007).
8. Suresh, S., Venkitaraj, K. P., Selvakumar, P. & Chandrasekar, M. Synthesis of Al2O3–Cu/water hybrid nanofluids using two step method and its thermo physical properties. *Colloids Surf. A* **388**(1–3), 41–48 (2011).
9. Waqas, M. *et al.* Magnetohydrodynamic (MHD) mixed con-vection flow of micropolar liquid due to nonlinear stretched sheet with convective condition. *Int. J. Heat Mass Transf.* **102**, 766–772 (2016).
10. Asghar, Z., Ali, N., Ahmed, R., Waqas, M. & Khan, W. A. A mathematical framework for peristaltic flow analysis of non-Newtonian Sisko fluid in an undulating porous curved channel with heat and mass transfer effects. *Comput. Methods Progr. Biomed.* **182**, 105040 (2019).
11. Waqas, M. A mathematical and computational framework for heat transfer analysis of ferromagnetic non-Newtonian liquid subjected to heterogeneous and homogeneous reactions. *J. Magn. Magn. Mater.* **493**, 165646 (2020).
12. Sohail, M. & Naz, R. Modified heat and mass transmission models in the magnetohydrodynamics flow of Sutterby nanofluid in stretching cylinder. *Phys. A* **549**, 124088 (2020).
13. Vajjha, R. S. & Das, D. K. Experimental determination of thermal conductivity of three nanofluids and development of new cor-relations. *Int. J. Heat Mass Transf.* **52**(21–22), 4675–4682 (2009).
14. Timofeeva, E. V., Routbort, J. L. & Singh, D. Particle shape effects on thermophysical properties of alumina nanoflu-ids. *J. Appl. Phys.* **106**(1), 014304 (2009).
15. Siddiqui, A. M., Mahmood, R. & Ghori, Q. K. Thin film flow of a third grade fluid on a moving belt by He's homotopy perturbation method. *Int. J. Nonlinear Sci. Numer. Simul.* **7**(1), 7–14 (2006).
16. Khaled, A. R. & Vafai, K. Hydromagnetic squeezed flow and heat transfer over a sensor surface. *Int. J. Eng. Sci.* **42**(5–6), 509–519 (2004).
17. Bilal, S., Sohail, M., Naz, R., Malik, M. Y. & Alghamdi, M. Upshot of ohmically dissipated Darcy-Forchheimer slip flow of mag-netohydrodynamic Sutterby fluid over radiating linearly stretched surface in view of Cash and Carp method. *Appl. Math. Mech.* **40**(6), 861–876 (2019).
18. Marzougui, S. *et al.* Entropy generation on magne-to-convective flow of copper–water nanofluid in a cavity with chamfers. *J. Therm. Anal. Calorim.* **143**(3), 2203–2214 (2021).
19. Gowda, R. P., Kumar, R. N., Prasannakumara, B. C., Nagaraja, B. & Gireesha, B. J. Exploring magnetic dipole contribution on ferromagnetic nanofluid flow over a stretching sheet: An application of Stefan blowing. *J. Mol. Liq.* **335**, 116215 (2021).
20. Sohail, M., Chu, Y. M., El-Zahar, E. R., Nazir, U. & Naseem, T. Contribution of joule heating and viscous dissipation on three dimensional flow of Casson model comprising temperature dependent conductance utilizing shooting method. *Phys. Scr.* **96**(8), 085208 (2021).
21. Naseem, T., Nazir, U., El-Zahar, E. R., Algelany, A. M. & Sohail, M. Numerical computation of Dufour and Soret effects on radiated material on a porous stretching surface with temperature-dependent thermal conductivity. *Fluids* **6**(6), 196 (2021).

22. Punith Gowda, R. J., Naveen Kumar, R., Jyothi, A. M., Prasannakumara, B. C. & Sarris, I. E. Impact of binary chemical reaction and activation energy on heat and mass transfer of marangoni driven boundary layer flow of a non-Newtonian nanofluid. *Processes* **9**(4), 702 (2021).

23. Jamshed, W., Nisar, K. S., Gowda, R. P., Kumar, R. N. & Prasannakumara, B. C. Radiative heat transfer of second grade nanofluid flow past a porous flat surface: a single-phase mathematical model. *Phys. Scr.* **96**(6), 064006 (2021).

24. Xiong, P. Y. *et al.* Dynamics of multiple solutions of Darcy-Forchheimer saturated flow of Cross nanofluid by a vertical thin needle point. *Eur. Phys. J. Plus* **136**(3), 1–22 (2021).

25. Gowda, R. P. *et al.* Computational modelling of nanofluid flow over a curved stretching sheet using Koo-Kleinstreuer and Li (KKL) correlation and modified Fourier heat flux model. *Chaos Solitons Fract.* **145**, 110774 (2021).

26. Gnaneswara Reddy, M., Punith Gowda, R. J., Naveen Kumar, R., Prasannakumara, B. C. & Ganesh Kumar, K. Analysis of modified Fourier law and melting heat transfer in a flow involving carbon nanotubes. *Proc. Inst. Mech. Eng. Part E J. Process Mech. Eng.* **235**(5), 1259–1268 (2021).

27. Varun Kumar, R. S., Gunderi Dhananjaya, P., Naveen Kumar, R., Punith Gowda, R. J. & Prasannakumara, B. C. Modeling and theoretical investigation on Casson nanofluid flow over a curved stretching surface with the influence of magnetic field and chemical reaction. *Int. J. Comput. Methods Eng. Sci. Mech.* **23**(1), 12–19 (2022).

28. Gowda, R. J., Kumar, R. N., Rauf, A., Prasannakumara, B. C. & Shehzad, S. A. Magnetized flow of sutterby nanofluid through cattaneo-christov theory of heat diffusion and stefan blowing condition. *Appl. Nanosci.* **2021**, 1–10 (2021).

29. Zhou, S. S. *et al.* Nonlinear mixed convective Williamson nanofluid flow with the suspension of gyrotactic microorganisms. *Int. J. Mod. Phys. B* **35**(12), 2150145 (2021).

30. Punith Gowda, R. J., Naveen Kumar, R., Jyothi, A. M., Prasannakumara, B. C. & Nisar, K. S. KKL correlation for simulation of nanofluid flow over a stretching sheet considering magnetic dipole and chemical reaction. *ZAMM-J. Appl. Math. Mech.* **101**(11), e202000372 (2021).

31. Shoaib, M. *et al.* Ohmic heating effects and entropy generation for nanofluidic system of Ree-Eyring fluid: Intelligent computing paradigm. *Int. Commun. Heat Mass Transfer* **129**, 105683 (2021).

32. Jyothi, A. M., Kumar, R. N., Gowda, R. P. & Prasannakumara, B. C. Significance of Stefan blowing effect on flow and heat transfer of Casson nanofluid over a moving thin needle. *Commun. Theor. Phys.* **73**(9), 095005 (2021).

33. Naseem, T. *et al.* Numerical exploration of thermal transport in water-based nanoparticles: A computational strategy. *Case Stud. Therm. Eng.* **27**, 101334 (2021).

34. Irandoost Shahrestani, M., Maleki, A., Safdari Shadloo, M. & Tlili, I. Numerical investigation of forced convective heat transfer and performance evaluation criterion of Al2O3/water nanofluid flow inside an axisymmetric microchan-nel. *Symmetry* **12**(1), 120 (2020).

35. Waini, I., Ishak, A. & Pop, I. Nanofluid flow on a shrinking cylinder with Al2O3 nanoparticles. *Mathematics* **9**(14), 1612 (2021).

36. Afridi, M. I., Tlili, I., Goodarzi, M., Osman, M. & Khan, N. A. Irreversibility analysis of hybrid nanofluid flow over a thin needle with effects of energy dissipation. *Symmetry* **11**(5), 663 (2019).

37. Abbas, T., Ayub, M., Bhatti, M. M., Rashidi, M. M. & Ali, M. E. S. Entropy generation on nanofluid flow through a hor-izontal Riga plate. *Entropy* **18**(6), 223 (2016).

38. Shankaralingappa, B. M., Prasannakumara, B. C., Gireesha, B. J. & Sarris, I. E. The impact of Cattaneo-Christov double diffusion on Oldroyd-B Fluid flow over a stretching sheet with thermophoretic particle deposition and relaxation chemical reaction. *Inventions* **6**(4), 95 (2021).

39. Shankaralingappa, B. M., Gireesha, B. J., Prasannakumara, B. C. & Nagaraja, B. Darcy-Forchheimer flow of dusty tangent hyperbolic fluid over a stretching sheet with Cattaneo-Christov heat flux. *Waves Random Complex Media* **2021**, 1–20 (2021).

40. Sarada, K., Gowda, R. J. P., Sarris, I. E., Kumar, R. N. & Prasannakumara, B. C. Effect of magnetohydrodynamics on heat transfer behaviour of a non-Newtonian fluid flow over a stretching sheet under local thermal non-equilibrium condition. *Fluids* **6**(8), 264 (2021).

41. Soumya, D. O., Gireesha, B. J., Venkatesh, P. & Alsulami, M. D. Effect of NP shapes on Fe3O4–Ag/kerosene and Fe3O4–Ag/water hybrid nanofluid flow in suction/injection process with nonlinear-thermal-radiation and slip condition; Hamilton and Crosser's model. *Waves Random Complex Media* **2022**, 1–22 (2022).

42. Ramesh, G. K., Madhukesh, J. K., Das, R., Shah, N. A. & Yook, S. J. Thermodynamic activity of a ternary nanofluid flow passing through a permeable slipped surface with heat source and sink. *Waves Random Complex Media* **2022**, 1–21 (2022).

43. Ramesh, G. K., Madhukesh, J. K., Shehzad, S. A. & Rauf, A. Ternary nanofluid with heat source/sink and porous medium effects in stretchable convergent/divergent channel. *Proc. Inst. Mech. Eng. Part E J. Process Mech. Eng.* https://doi.org/10.1177/0954408922 1081344 (2022).

44. Kotresh, M. J., Ramesh, G. K., Shashikala, V. K. R. & Prasannakumara, B. C. Assessment of Arrhenius activation energy in stretched flow of nanofluid over a rotating disc. *Heat Transfer* **50**(3), 2807–2828 (2021).

45. Madhukesh, J. K., Ramesh, G. K., Alsulami, M. D. & Prasannakumara, B. C. Characteristic of thermophoretic effect and convective thermal conditions on flow of hybrid nanofluid over a moving thin needle. *Waves Random Complex Media* **2021**, 1–23 (2021).

46. Li, J., Liu, L., Zheng, L. & Bin-Mohsin, B. Unsteady MHD flow and radiation heat transfer of nanofluid in a finite thin film with heat generation and thermophoresis. *J. Taiwan Inst. Chem. Eng.* **67**, 226–234 (2016).

47. Wang, C. Analytic solutions for a liquid film on an unsteady stretching surface. *Heat Mass Transf.* **42**(8), 759–766 (2006).

48. Abel, M. S., Mahesha, N. & Tawade, J. Heat transfer in a liquid film over an unsteady stretching surface with viscous dissipation in presence of external magnetic field. *Appl. Math. Model.* **33**(8), 3430–3441 (2009).

Author contributions

All authors reviewed the manuscript.

Funding

Competing interests

The authors declare no competing interests.

Additional information

Correspondence and requests for materials should be addressed to M.S. or M.R.A.

Reprints and permissions information is available at www.nature.com/reprints.

Publisher's note Springer Nature remains neutral with regard to jurisdictional claims in published maps and institutional affiliations.